*Proceedings of the*
*Annual Stability Conference*
*Structural Stability Research Council*
*Pittsburgh, Pennsylvania, May 10-14, 2011*

# Impact of cross-section stability on cold-formed steel member stiffness and ductility

D. Ayhan[1], B. W. Schafer[2]

## Abstract

The objective of this paper is to provide work towards design methods to predict both the loss of stiffness and the available ductility for cold-formed steel members subject to cross-section deformations resulting from local and distortional buckling. Existing design specifications provide some guidance on how to predict the stiffness of cold-formed steel members, but no guidance on their available ductility. Further, the guidance on stiffness is limited, particularly for distortional buckling, and largely has not been validated against testing. The long-term goal of the research is to improve modern seismic design of cold-formed steel members. Existing four point bending tests on cold-formed steel lipped channel and lipped zee beams failing in local and distortional buckling, are used as the basis for the study conducted herein. The experimental results are converted from load-displacement to moment-rotation and simplified into multi-linear response curves. Stiffness of the conducted tests up to the peak load (moment) is compared with predictions based on the effective width method and the direct strength method. Relationships between local and distortional cross-section slenderness and the observed and predicted secant stiffness up to the peak load are examined. To explore models that include energy dissipation and post-peak behavior, as required for modern seismic design, simple hysteretic models are fit to the full response curve generated from the experimental data; including, an equivalent energy elastic plastic model, and an equivalent energy model that incorporates the pre-peak stiffness reductions predicted by current design methods. Relationships between local and distortional cross-section slenderness and the developed ductility parameters are explored. Formalization of a predictive method for the ductility parameters is underway, as is expansion of the database of studied sections through nonlinear finite element analysis.

[1] Visiting Student Scholar, Johns Hopkins University <dayhan1@jhu.edu>, and Ph.D. Candidate, Istanbul Technical University, <ayhan@itu.edu.tr>
[2] Professor and Chair, Department of Civil Engineering, Johns Hopkins University, <schafer@jhu.edu>

## 1. Introduction

Cold-formed steel (CFS) is a popular building material enjoying a wide and growing base of applications in civil structures. Current design, essentially the world over, has focused on member-level strength prediction. A problem, for example in beams, complicated by the presence of material yielding, local buckling, distortional buckling, lateral-torsional buckling, and combinations thereof. Significantly less attention has been given to the issue of stiffness; however, design specifications (e.g., AISI-S100-07) do provide methods for approximating the reduced stiffness due to local buckling – typically using variations of the effective width method. In addition, AISI-S100-07 Appendix 1 also provides an approach for predicting the stiffness that relies directly on the cross-section slenderness. These stiffness reductions are only valid up to the ultimate strength of the member, and no means are provided for determining the stiffness past the peak strength.

Collapse analysis of a CFS building system (i.e. a building comprised of load bearing cold-formed steel framing), whether for static loads, wind loads, progressive collapse, or seismic design is predicated on knowledge of the nonlinear response of the components and connections that make up a building. Simple determination of the force or moment redistribution in a CFS building system after one member fails may not be accurately completed with current knowledge, requiring current design to ignore system effects and instead concentrate on first member failure only. Given that CFS cross-sections are typically locally slender they have a more complicated and less forgiving $M$-$\theta$ response than compact hot-rolled steel beams.

Further, since much of the nonlinear response in CFS building systems is related to the connections, CFS member response has not been pursued in much detail. Regardless this lack of understanding has consequences. For example, in CFS seismic design, buildings are detailed with the goal of concentrating all nonlinear response in pre-tested shearwalls. The capacity of other members (or connections) to absorb any of the deformation (energy) is ignored – as is the potential for redistribution of forces – leading to model predictions divorced from reality and structural systems that do not achieve full economy.

The objective of this paper is to begin the exploration of, and prediction for, the nonlinear response ($M$-$\theta$) of cold-formed steel members. Existing tests on cold-formed steel beams in local and distortional buckling are used as the basis for this initial study. The data is processed and stiffness and ductility examined.

## 2. Local and distortional buckling of cold-formed steel beams

The moment-rotation response of beams is known to be highly sensitive to the cross-section slenderness. For typical CFS beams (lipped channels and lipped zees) the buckling modes of local and distortional buckling must be considered in addition to lateral-torsional buckling. Here we focus on existing experiments on beams in local and distortional buckling.

### *2.1 Existing Experimental Data*

The experiments on local and distortional buckling of CFS beams by Yu and Schafer (2003, 2006, and 2007) are utilized herein. The test setup, typical failure modes, strength, and response of the tested specimens are summarized in Fig. 1. The tests consisted of paired CFS beams tested in 4 point bending.

(a) local test setup

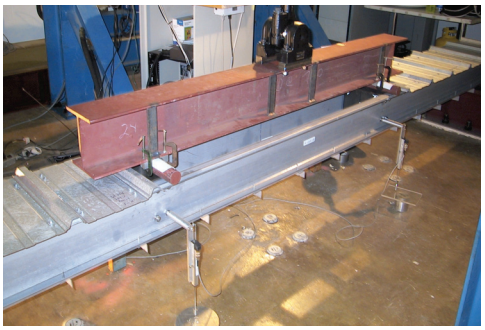

(b) distortional test setup

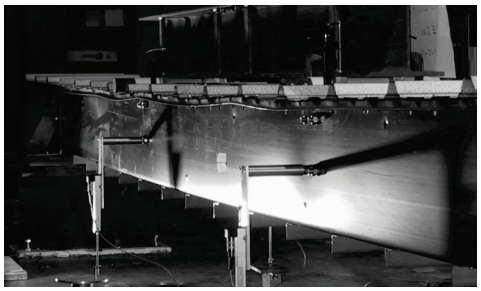

(c) local test at failure

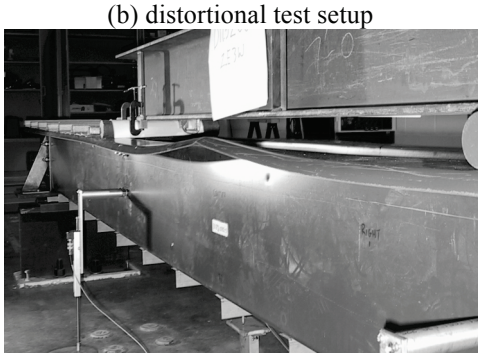

(d) distortional test at failure

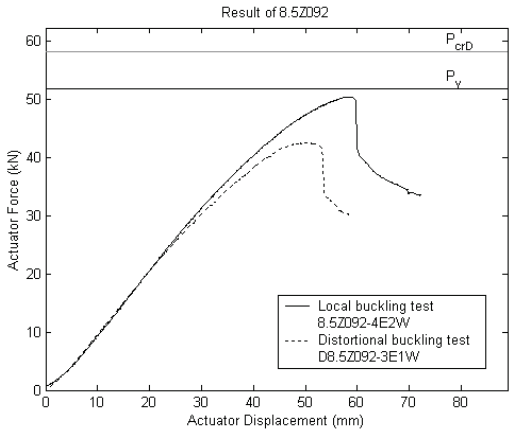


(e) local vs. distortional response for identical specimens

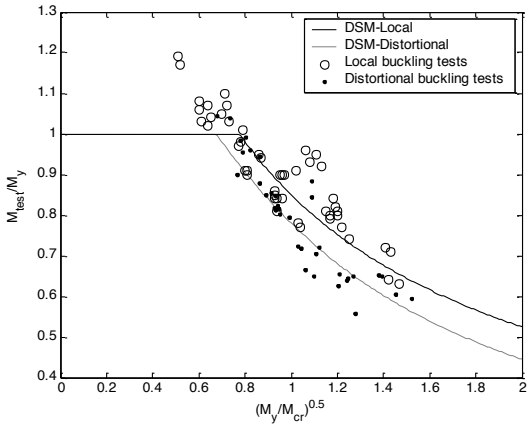


(f) correlation of strength to cross-section slenderness

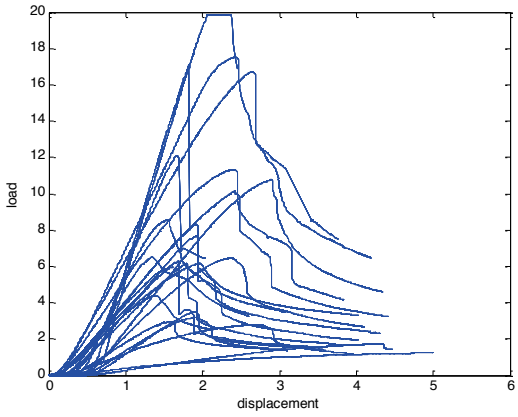


(g) load-displacement response of local tests

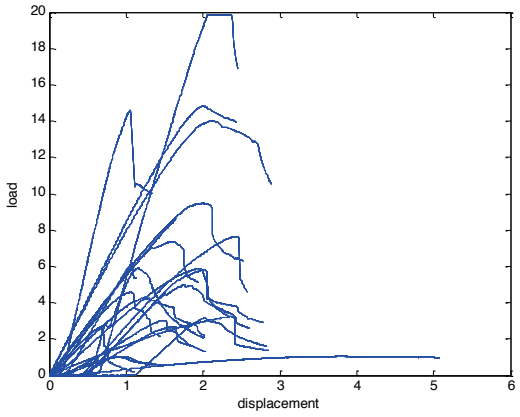


(h) load-displacement response of distortional tests

Figure 1: Local and distortional buckling tests of Yu and Schafer (Note, (a), (b) Yu and Schafer (2007), (c)-(f) Yu and Schafer 2006, (g),(h) original to this paper)

In the local buckling tests a corrugated metal panel was attached to the compression flange in the moment span to insure distortional buckling was restricted (Fig. 1a,c). In the distortional buckling tests the panel remained in the shear spans only and no restraint was provided to the compression flange of the specimens (Fig. 1b,d) Tests were carried out on industry standard lipped channel and lipped zee specimens varying from 92 to 305 mm (3.62 to 12 in.) deep and from 1.09 to 2.46 mm (0.043 to 0.097 in.) thick.

Members failing in distortional buckling typically exhibited lower capacities and a slight decrease in stiffness prior to the peak strength as shown in Fig. 1e. The peak strength observed in the tests correlated well with cross-section slenderness and the independently determined direct strength method design expressions for local and distortional buckling (AISI-S100-07 Appendix 1), as shown in Fig. 1f.

*2.2 Conversion of recorded data*

Working from the raw data, twenty-four of the local buckling tests (Fig. 1g) and twenty-two of the distortional buckling tests (Fig. 1h) from Yu and Schafer (2003, 2006) were employed in this study. The raw data was down-sampled to 10 pre-peak points, each one in increments of 10% of the displacement at peak strength, as shown in Fig. 2a. Based on the force levels corresponding to 10% pre-peak displacement increments, post-peak data was determined. Due to the low density of available data immediately after the peak strength a 3rd order polynomial was fit to the post-peak strength and results from that polynomial provided the down-sampled post-peak data, as shown in Fig. 2a.

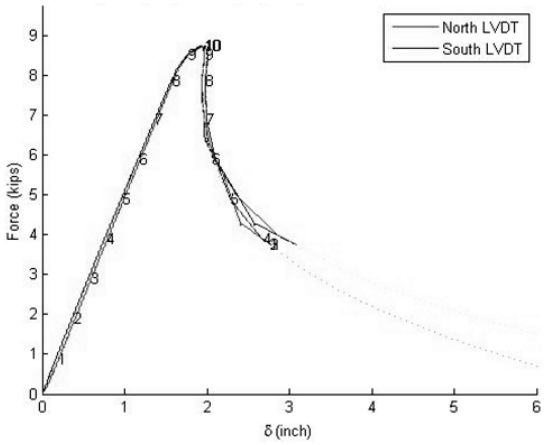


(a) digitized points (1-10) shown for 8.5Z120-3E2W

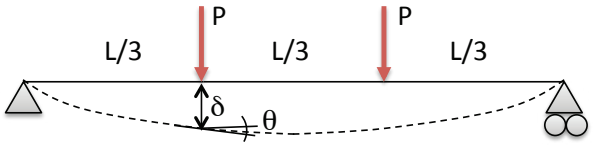


(b) variable definitions and continuous model

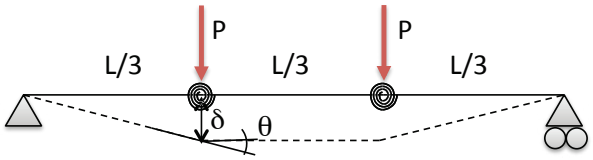


(c) two parameter lumped rotational spring model

Figure 2: Conversion of measured data in 4 point bending test

Force measurements are recorded in the load cell in the actuator (see center of the spreader beam Fig. 1b) and displacement measurements from LVDTs at the load points (e.g., see Fig. 1c). Note, specimens are made up of two cold-formed steel beams in parallel, thus the moment of inertia for the beam in Fig. 2b is equal to the summation of the moment of inertia for the two beams. Conversion of the measured test data to stiffness as well as moment-rotation is as follows:

test: $\delta$ = average of LVDTs positioned under two loading points
$P$ = ½ of force measured from load cell
$k = P/\delta$

$\theta = \delta/(L/3)$
$M = P(L/3)$
$k_\theta = M/\theta$

The rotation determined from the test data is approximate, and is consistent with the lumped parameter model of Fig. 2c. For comparison, linear elastic analysis using beam theory (ignoring cross-section deformation), provides the following solution:

elastic: $\delta_e = 5PL^3/(162EI)$
$k_e = 162EI/(5L^3)$
$\theta_e = PL^2/(18EI)$
$k_\theta = 6EI/L$
also note:
$\delta_e/(L/3) = 15PL^2/(162EI)$

The preceding are used to compare observed displacements to expected (analytical) displacements and provide information towards development of a lumped stiffness model (Fig. 2c) that may eventually be used in nonlinear collapse analysis.

**3. Cold Formed Steel Member Stiffness (pre-peak)**

For strength, comparisons between the effective width method (EWM) and the Direct Strength Method (DSM) may be found elsewhere (see, e.g., Schafer 2006, Ziemian 2010). However, little in the way of validation or comparison has been provided for the stiffness predictions of the two methods.

*3.1 Prediction based on Effective Width Method*

Stiffness prediction by the effective width method (as implemented in the main Specification of AISI-S100-07) may be understood as follows. The effective moment of inertia ($I_{e\text{-}EWM}$) is calculated from appropriate summation of the effective widths of all the elements:

$$I_{e-EWM} = \sum_{elements} y_e^2 b_e t$$

where $y_e$ is the distance from the effective neutral axis to the effective centroid of the element, $t$ is the thickness, and $b_e$ is the effective width of a given element, determined from:

$$b_e = \begin{cases} b\left(1 - 0.22\sqrt{f_{cr}/f}\right)\sqrt{f_{cr}/f} & \text{if } \sqrt{f/f_{cr}} > 0.673 \\ b & \text{if } \sqrt{f/f_{cr}} \le 0.673 \end{cases}$$

where $b$ is the gross element width, $f_{cr}$ is the elastic local buckling stress of the element (see Chapter B of AISI-S100-07) and $f$ is the applied stress at which the effective moment of inertia is to be determined. Note, $f=M/S_g$, where M is the applied moment at which the effective moment of inertia is to be determined and $S_g$ is the gross section modulus. An interesting feature of the EWM for stiffness determination is that the location in the cross-section is significant for determining the reduced stiffness, i.e., large effective width reductions in the flange result in large reductions in $I_{e\text{-}EWM}$ while large reductions in the web do not.

In this study, CFS (2010), a comprehensive general-purpose cold-formed steel component design tool, is used to calculate effective section properties.

*3.2 Prediction based on Direct Strength Method*

Stiffness prediction by the Direct Strength Method (as implemented in Appendix 1 of AISI-S100-07) assumes that the stiffness reduction follows the same trends as the strength reduction predicted by DSM. Thus, for local buckling the effective moment of inertia ($I_{e\ell-DSM}$) is determined as follows:

$$I_{e\ell-DSM} = \begin{cases} I_g\left(1-0.15(M_{cr\ell}/M)^{0.4}\right)(M_{cr\ell}/M)^{0.4} & \text{if } \sqrt{M/M_{cr\ell}} > 0.776 \\ I_g & \text{if } \sqrt{M/M_{cr\ell}} \le 0.776 \end{cases}$$

where $I_g$ is the gross moment of inertia, $M_{cr\ell}$ is the elastic critical local buckling moment, and $M$ is the applied moment at which the effective stiffness is to be determined. Note, AISI-S100-07 Appendix 1 does not provide the explicit formula above, but it may be arrived at with appropriate substitutions. DSM treats stiffness loss due to distortional buckling in a similar manner:

$$I_{ed-DSM} = \begin{cases} I_g\left(1-0.22\sqrt{M_{crd}/M}\right)\sqrt{M_{crd}/M} & \text{if } \sqrt{M/M_{crd}} > 0.673 \\ I_g & \text{if } \sqrt{M/M_{crd}} \le 0.673 \end{cases}$$

where $M_{crd}$ is the elastic critical distortional buckling moment and other terms ($I_g$, $M$) are the same as for local buckling. Note, the EWM as implemented in AISI-S100-07 currently includes no stiffness loss in distortional buckling – so this predictive equation is unique to DSM. Validation of either the EWM or DSM stiffness predictions is scarce.

*3.3 Evaluation of test results*

*3.3.1 Tangent stiffness*

Utilizing the data of Fig. 1g and h, and following the conversion methodology outlined in Section 2.2 the tangent stiffness was determined throughout the tests. The tangent stiffness ($k_{tan}$) was normalized by the elastic stiffness ($k_e$) and the results are provided in Fig. 3.

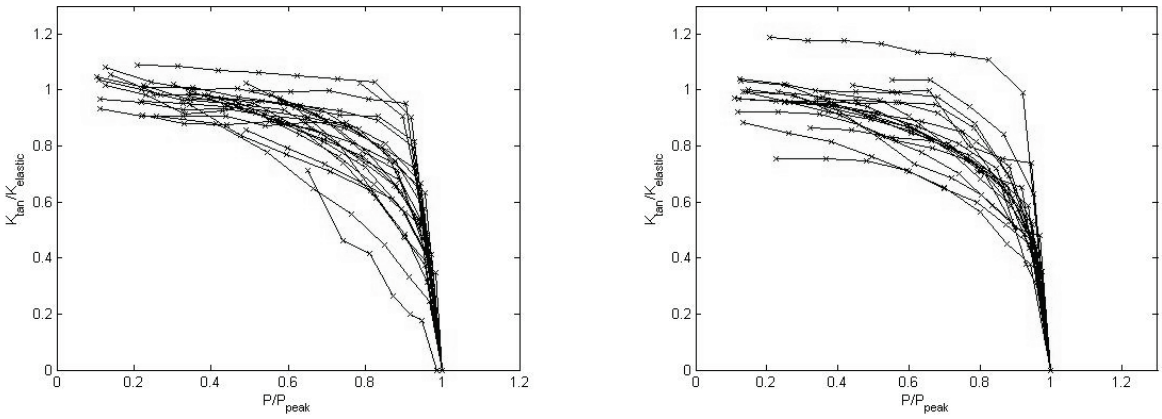


(a) local buckling tests (b) distortional buckling tests

Figure 3: Normalized tangent stiffness as a function of load

In general the initial stiffness is in good agreement with the elastic stiffness ($k/k_e$ values in Fig. 3 are near 1 under small load); however, the agreement is better for the local buckling tests than the distortional buckling tests. The tangent stiffness at peak strength is, by definition, zero – as a result the stiffness drops precipitously as the load approaches the peak strength. The reduced (effective) moment of inertia provided in Section 3.2 for EWM and DSM are for the secant, not the tangent stiffness, thus the secant stiffness is explored in the following section.

*3.3.2 Secant stiffness*

The secant stiffness for all available tests data is calculated and reported in Table 1. As Fig. 3 indicates and Fig. 1g and h show, the data has some uncertainty associated with it. First, in most tests some initial accommodation of the testing fixtures was required before the linear elastic regime initiated. This results in initial stiffness predictions significantly below elastic analysis predictions; however, under a small amount of load – typically on the order of 20% of the peak load, the linear elastic regime is observed. In the analysis presented herein these initial results during the accommodation phase were discarded (they are indicated in italics in Table 1.)

Secant stiffness values were calculated for the EWM and DSM methods per Section 3.1 and 3.2 and compared against the measured values in Figure 4. In Figure 4 the horizontal axis is the cross-section slenderness (either local or distortional). As the moment increases the cross-section slenderness increases and the predictive methods proceed from fully effective to partially effective and the stiffness reduces. Neither the EWM or the DSM method for reducing the stiffness ($I_e$) follows the same "shape" as the test data as the section stiffness reduces.

The EWM provides cross-section specific predictions of the reduced stiffness. The reductions initiate earlier and are more severe than the observed stiffness reductions. The DSM method provides a singular prediction as a function of cross-section slenderness – so all sections reduce stiffness in the same manner. The predicted DSM reductions follow the mean of observed stiffness, but much scatter remains. The EWM reductions generally follow the same shape as the DSM reductions. The DSM reductions provide an upperbound to the EWM reductions.

A statistical summary comparing EWM and DSM to the measured data is provided in Table 2. The test-to-predicted ratio for the reduced moment of inertia is compared at the ten load levels explored. Focusing on predicting the secant stiffness at peak strength, DSM provides a mean test-to-predicted stiffness ratio of 0.97 for both the local and distortional buckling tests and a coefficient of variation of 15% for local buckling and 21% for distortional buckling; while EWM provides a mean test-to-predicted stiffness ratio of 1.13 in local buckling, 1.03 in distortional buckling and coefficients of variation of 18 and 20% respectively. Neither method provides highly accurate stiffness predictions, but DSM is superior in terms of mean and variance; therefore, it seems reasonable to conclude that either method may be used and DSM's simplicity may make it more advantageous in many situations.

Table 1: Secant stiffness values from tests of Yu and Schafer (2003, 2006, 2007)

(a) local buckling tests

| Specimen | $k_{elastic}$ | kN_01 | kN_02 | kN_03 | kN_04 | kN_05 | kN_06 | kN_07 | kN_08 | kN_09 | kN_test |
|---|---|---|---|---|---|---|---|---|---|---|---|
| 8.5Z120-3E2W-21 | 4.899 | *4.389* | *4.775* | *4.879* | *4.920* | *4.948* | *4.956* | 4.968 | 4.956 | 4.775 | 4.418 |
| 8.5Z105-2E1W | 4.339 | *5.448* | 4.672 | 4.551 | 4.486 | 4.420 | 4.380 | 4.307 | 4.198 | 4.053 | 3.825 |
| 8.5Z092-4E2W | 3.725 | 4.072 | 3.936 | 3.850 | 3.770 | 3.672 | 3.562 | 3.434 | 3.295 | 3.126 | 2.922 |
| 8.5Z082-1E2W | 3.347 | 3.840 | 3.434 | 3.282 | 3.207 | 3.122 | 3.024 | 2.930 | 2.834 | 2.727 | 2.607 |
| 8.5Z073-4E3W | 3.049 | 3.007 | 2.946 | 2.915 | 2.908 | 2.879 | 2.859 | 2.841 | 2.800 | 2.752 | 2.673 |
| 8.5Z073-1E2W | 3.043 | 2.875 | 2.827 | 2.811 | 2.811 | 2.779 | 2.758 | 2.752 | 2.735 | 2.698 | 2.568 |
| 8.5Z065-3E1W | 2.639 | 2.987 | 2.873 | 2.798 | 2.760 | 2.730 | 2.691 | 2.641 | 2.580 | 2.504 | 2.359 |
| 8.5Z059-4E3W | 2.402 | 2.446 | 2.463 | 2.412 | 2.386 | 2.378 | 2.355 | 2.334 | 2.318 | 2.295 | 2.228 |
| 8.5Z059-2E1W | 2.416 | 2.826 | 2.616 | 2.512 | 2.425 | 2.400 | 2.378 | 2.367 | 2.346 | 2.318 | 2.254 |
| 8C097-2E3W | 2.834 | *2.433* | *2.662* | *2.745* | 2.760 | 2.757 | 2.734 | 2.691 | 2.612 | 2.498 | 2.341 |
| 8C068-4E5W | 2.256 | *1.755* | *1.938* | *2.017* | *2.063* | 2.069 | 2.047 | 2.013 | 1.955 | 1.883 | 1.773 |
| 8C068-1E2W | 2.240 | *1.830* | *1.999* | *2.056* | 2.091 | 2.089 | 2.065 | 2.023 | 1.975 | 1.908 | 1.808 |
| 8C054-1E8W | 1.642 | *1.413* | 1.468 | 1.462 | 1.459 | 1.457 | 1.456 | 1.450 | 1.427 | 1.393 | 1.323 |
| 8C043-5E6W | 1.499 | *1.171* | *1.330* | *1.372* | *1.392* | 1.398 | 1.383 | 1.353 | 1.317 | 1.273 | 1.185 |
| 8C043-3E1W | 1.448 | *1.096* | *1.096* | *1.194* | *1.233* | *1.271* | 1.291 | 1.289 | 1.261 | 1.226 | 1.14 |
| 12C068-9E5W | 5.140 | *3.196* | *2.922* | *3.895* | 4.058 | 4.045 | 4.020 | 3.945 | 3.833 | 3.623 | 3.396 |
| 12C068-3E4W | 5.291 | *2.880* | *2.880* | *3.826* | *4.204* | *4.329* | 4.363 | 4.320 | 4.225 | 4.047 | 3.782 |
| 10C068-2E1W | 2.923 | *2.721* | *2.794* | *2.835* | 2.855 | 2.809 | 2.754 | 2.631 | 2.509 | 2.430 | 2.226 |
| 6C054-2E1W | 0.934 | *0.697* | *0.736* | 0.781 | 0.774 | 0.755 | 0.723 | 0.689 | 0.649 | 0.609 | 0.567 |
| 4C054-1E2W | 0.309 | *0.251* | *0.263* | *0.268* | *0.279* | 0.281 | 0.276 | 0.267 | 0.256 | 0.241 | 0.227 |
| 3.62C054-1E2W-3 | 0.255 | *0.406* | *0.315* | 0.270 | 0.242 | 0.221 | 0.201 | 0.185 | 0.170 | 0.157 | 0.147 |
| 11.5Z092-1E2W | 9.455 | 10.349 | 10.255 | 10.270 | 10.278 | 10.264 | 10.199 | 10.187 | 10.101 | 10.029 | 9.806 |
| 11.5Z082-2E1W | 8.607 | *8.588* | *8.493* | *8.556* | 8.859 | 8.503 | 8.533 | 8.534 | 8.529 | 8.504 | 8.446 |
| 11.5Z073-2E1W | 7.177 | 6.721 | 6.721 | 6.770 | 6.770 | 6.750 | 6.737 | 6.707 | 6.617 | 6.470 | 6.216 |

(b) distortional buckling tests

| | $k_{elastic}$ | kN_01 | kN_02 | kN_03 | kN_04 | kN_05 | kN_06 | kN_07 | kN_08 | kN_09 | kN_peak |
|---|---|---|---|---|---|---|---|---|---|---|---|
| D8.5Z120-4E1W | 4.8993 | *4.701* | *4.866* | *4.885* | *4.921* | *4.976* | *4.949* | 4.961 | 4.877 | 4.766 | 4.503 |
| D8.5Z115-1E2W | 4.8447 | *4.519* | 4.62 | 4.595 | 4.538 | 4.473 | 4.388 | 4.295 | 4.147 | 3.972 | 3.693 |
| D8.5Z092-3E1W | 3.6877 | *3.487* | *3.515* | 3.525 | 3.515 | 3.459 | 3.393 | 3.305 | 3.189 | 3.043 | 2.81 |
| D8.5Z082-4E3W | 3.4129 | *2.909* | *3.138* | *3.127* | 3.195 | 3.151 | 3.105 | 3.035 | 2.95 | 2.706 | 2.51 |
| D8.5Z065-4E3W | 2.6868 | 2.677 | 2.661 | 2.622 | 2.586 | 2.558 | 2.518 | 2.47 | 2.339 | 2.171 | 2.013 |
| D8.5Z065-1E2W-2 | 2.5367 | *2.44* | *2.461* | *2.468* | 2.482 | 2.49 | 2.489 | 2.47 | 2.424 | 2.299 | 2.196 |
| D8.5Z059-1W2E | 2.6327 | *1.872* | *1.981* | *2.09* | *2.133* | 2.16 | 2.155 | 2.152 | 2.133 | 2.051 | 1.951 |
| D11.5Z092-1E2W | 8.6959 | *10.15* | *10.15* | 10.27 | 10.25 | 10.22 | 10.19 | 10.12 | 10.09 | 10.02 | 9.796 |
| D11.5Z082-5E4W | 8.1795 | *7.908* | 7.931 | 7.924 | 7.874 | 7.899 | 7.878 | 7.829 | 7.673 | 7.351 | 7.007 |
| D8C097-5E4W | 2.954 | 2.821 | 2.743 | 2.743 | 2.717 | 2.67 | 2.626 | 2.575 | 2.524 | 2.456 | 2.362 |
| D8C085-2E1W | 2.5243 | *2.277* | *2.277* | *2.342* | 2.363 | 2.35 | 2.318 | 2.246 | 2.167 | 2.07 | 1.959 |
| D8C068-6E7W | 2.0966 | 2.143 | 2.143 | 2.116 | 2.069 | 2.024 | 1.981 | 1.923 | 1.859 | 1.782 | 1.669 |
| D8C054-7E6W | 1.5856 | *1.613* | *1.613* | 1.659 | 1.613 | 1.613 | 1.597 | 1.606 | 1.578 | 1.536 | 1.461 |
| D8C045-1E2W | 1.116 | *0.865* | *0.799* | 0.865 | 0.849 | 0.839 | 0.821 | 0.808 | 0.774 | 0.739 | 0.705 |
| D8C043-4E2W | 1.4202 | *1.323* | *1.345* | *1.352* | 1.366 | 1.366 | 1.359 | 1.348 | 1.318 | 1.262 | 1.195 |
| D8C033-1E2W | 1.0748 | 1.22 | 1.144 | 1.093 | 1.049 | 1.007 | 0.979 | 0.937 | 0.906 | 0.856 | 0.816 |
| D12C068-10E11W | 5.2217 | 5.398 | 5.243 | 5.191 | 5.026 | 4.889 | 4.747 | 4.565 | 4.436 | 4.143 | 3.835 |
| D12C068-1E2W | 5.2978 | *3.096* | *2.913* | *3.096* | *3.162* | *3.254* | *3.306* | *3.276* | *3.352* | 3.446 | 3.38 |
| D10C068-4E3W | 3.2962 | 3.022 | 2.988 | 2.908 | 2.833 | 2.747 | 2.667 | 2.59 | 2.498 | 2.396 | 2.287 |
| D10C056-3E4W | 3.0011 | *2.744* | *2.818* | 2.81 | 2.793 | 2.783 | 2.744 | 2.681 | 2.591 | 2.488 | 2.337 |
| D6C063-2E1W | 0.8649 | *0.887* | *0.898* | *0.887* | 0.937 | 0.865 | 0.847 | 0.818 | 0.79 | 0.759 | 0.721 |
| D3.62C054-3E4W | 0.2491 | 0.473 | 0.405 | 0.349 | 0.312 | 0.284 | 0.262 | 0.241 | 0.222 | 0.204 | 0.187 |

Notes: stiffness reported in kN/mm, see Fig. 2a for designation of 10 pre_peak points

*Italicized* values are less than elastic (analytical) prediction and discarded based on shape of load-displacement curve (i.e. are due to accommodation of testing fixtures)

Shaded values are regions where $I_e$ by DSM predicts a reduction in stiffness (i.e., $I_e < I_g$)

Specimen names are detailed in Yu and Schafer (2003, 2006), the first number is section depth in inches.

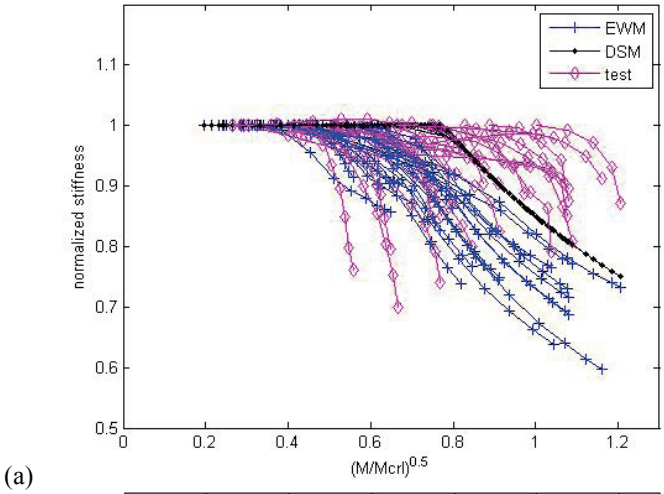


(a)

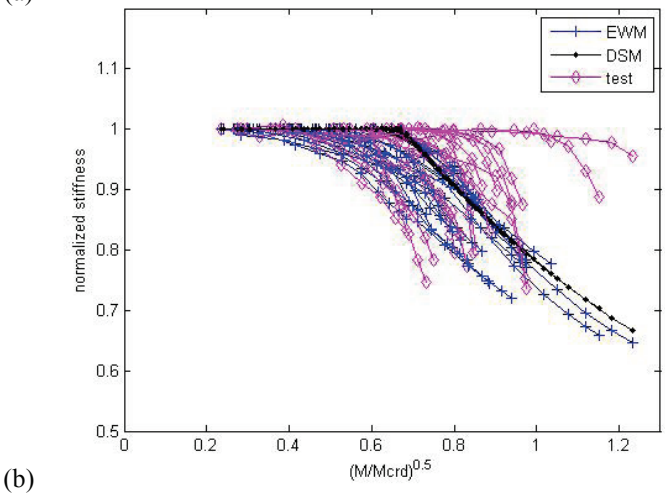


(b)

Figure 4: Comparison of DSM and EWM $I_{eff}$ results with (a) local and (b) distortional tests

Table 2: Summary of Test-to-Predicted Ratios for $I_{eff}$ by EWM and DSM

| | | $k_{secant\text{-}test}/k_{secant\text{-}predicted}$ at | | | | | | | | | |
|---|---|---|---|---|---|---|---|---|---|---|---|
| | | $\delta_{peak}$ | $0.9\delta_{peak}$ | $0.8\delta_{peak}$ | $0.7d_{peak}$ | $0.6\delta_{peak}$ | $0.5\delta_{peak}$ | $0.4\delta_{peak}$ | $0.3\delta_{peak}$ | $0.2\delta_{peak}$ | $0.1\delta_{peak}$ |
| ***LOCAL BUCKLING TESTS*** | | | | | | | | | | | |
| | n | 24 | 24 | 24 | 24 | 23 | 21 | 18 | 13 | 9 | 7 |
| DSM | μ | 0.97 | 1.01 | 1.02 | 1.02 | 1.01 | 0.99 | 0.98 | 0.98 | 0.99 | 1.00 |
| | CV | 0.15 | 0.13 | 0.12 | 0.09 | 0.07 | 0.03 | 0.02 | 0.01 | 0.01 | 0.00 |
| | min | 0.70 | 0.75 | 0.80 | 0.86 | 0.90 | 0.93 | 0.95 | 0.96 | 0.98 | 1.00 |
| | max | 1.19 | 1.23 | 1.25 | 1.23 | 1.18 | 1.06 | 1.00 | 1.00 | 1.00 | 1.00 |
| EWM | μ | 1.13 | 1.17 | 1.16 | 1.15 | 1.11 | 1.07 | 1.03 | 1.00 | 0.99 | 1.00 |
| | CV | 0.18 | 0.15 | 0.13 | 0.11 | 0.09 | 0.07 | 0.05 | 0.03 | 0.01 | 0.00 |
| | min | 0.77 | 0.83 | 0.88 | 0.92 | 0.96 | 0.98 | 0.96 | 0.96 | 0.98 | 1.00 |
| | max | 1.54 | 1.55 | 1.52 | 1.46 | 1.38 | 1.27 | 1.15 | 1.07 | 1.00 | 1.00 |
| ***DISTORTIONAL BUCKLING TESTS*** | | | | | | | | | | | |
| | n | 22 | 22 | 21 | 21 | 20 | 20 | 18 | 14 | 9 | 7 |
| DSM | μ | 0.97 | 1.00 | 1.01 | 1.01 | 0.99 | 0.98 | 0.97 | 0.96 | 0.97 | 1.00 |
| | CV | 0.21 | 0.19 | 0.18 | 0.16 | 0.14 | 0.11 | 0.08 | 0.06 | 0.04 | 0.00 |
| | min | 0.43 | 0.46 | 0.50 | 0.53 | 0.57 | 0.62 | 0.68 | 0.76 | 0.88 | 1.00 |
| | max | 1.43 | 1.42 | 1.37 | 1.31 | 1.25 | 1.18 | 1.10 | 1.01 | 1.01 | 1.00 |
| EWM | μ | 1.03 | 1.06 | 1.07 | 1.07 | 1.04 | 1.02 | 0.99 | 0.99 | 0.98 | 1.00 |
| | CV | 0.20 | 0.19 | 0.17 | 0.15 | 0.13 | 0.11 | 0.08 | 0.06 | 0.04 | 0.00 |
| | min | 0.46 | 0.50 | 0.54 | 0.59 | 0.63 | 0.68 | 0.73 | 0.79 | 0.89 | 1.00 |
| | max | 1.48 | 1.46 | 1.41 | 1.36 | 1.29 | 1.20 | 1.10 | 1.04 | 1.02 | 1.01 |

Note: n=number of tests used, μ=average, CV=coefficient of variation

## 4. Cold Formed Steel Member Ductility

The tests of Yu and Schafer (2003, 2006, 2007) were monotonic and static; however a significant amount of the post-peak displacements were observed and recorded (see Fig. 1g and h). This data provides a means to examine the ductility of a wide variety of industry standard lipped channel and lipped zee sections. The load-displacement response was converted to moment-rotation following the "test" method defined in Section 2.2. In this section we seek simplified models that may be used to predict the full nonlinear response for utilization in nonlinear collapse analysis (both static and dynamic).

Variations of the Equivalent Energy Elastic Plastic (EEEP) method (Park 1988) were employed herein. The most basic model follows that commonly used in shearwall testing (e.g., Branston et al. 2006) where an elastic-perfectly plastic $M$-$\theta$ curve is found such that the energy under the $M$-$\theta$ curve equals the energy under the tested $M$-$\theta$ curve. The following variations were examined:

Bilinear models (Fig. 5a)

1st: Elastic up to $0.80M_{peak}$, plastic until $\theta_{max1}$, such that area under tested $M$-$\theta$ curve up to $0.8M_{postpeak}$ equated to the model

2nd: Elastic up to $M_{peak}$, plastic until $\theta_{max2}$, such that area under curves up to $0.8M_{postpeak}$ equated, also note in general $\theta_{max2}<\theta_{max1}$ (unless test $M$-$\theta$ is stiffening)

Trilinear models (Fig. 5b)

1st: Elastic up to fully effective moment, follow secant stiffness as determined by DSM based on $M_{peak}$ until moment reaches $0.8M_{peak}$, plastic until $\theta_{max1}$, such that area under curves up to $0.8M_{postpeak}$ equated

2nd: Elastic up to fully effective moment, follow secant stiffness as determined by DSM based on $M_{peak}$ until moment reaches $M_{peak}$, plastic until $\theta_{max2}$, such that area under curves up to $0.8M_{postpeak}$ equated ($\theta_{max2}<\theta_{max1}$)

Also a variation on both models where $0.5M_{postpeak}$ replaced $0.8M_{postpeak}$ was pursued. The resulting rotation parameters, for the studied models, are provided in Table 3. In some instances, due to the shape of the $M$-$\theta$ test curve no plastic region is possible. Further, when no stiffness reduction occurs prior to peak strength (rows of Table 1 with no shading denotes members with no predicted stiffness reduction) the bilinear and trilinear models are the same.

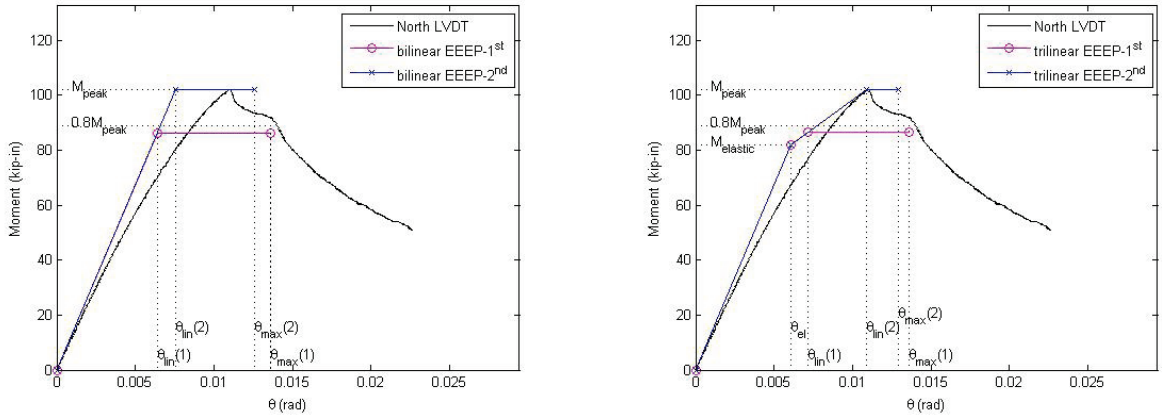


(a) bilinear EEEP models (b) trilinear EEEP models

Figure 5: Schematics and variable definitions for studied EEEP models

Table 3: Rotation parameters determined for variations of EEEP model formulation

(a) local buckling tests

| | EEEP-bilinear | | | | | | | | EEEP-trilinear | | | | | | | |
|---|---|---|---|---|---|---|---|---|---|---|---|---|---|---|---|---|
| | 1st | | | | 2nd | | | | 1st | | | | 2nd | | | |
| | 0.80F_peak | | 0.50F_peak | | 0.80F_peak | | 0.50F_peak | | 0.80F_peak | | 0.50F_peak | | 0.80F_peak | | 0.50F_peak | |
| | $\theta_{lin}$ | $\theta_{max}$ | $\theta_{lin}$ | $\theta_{max}$ | $\theta_{lin}$ | $\theta_{max}$ | $\theta_{lin}$ | $\theta_{max}$ | $\theta_{lin2}$ | $\theta_{max}$ | $\theta_{lin2}$ | $\theta_{max}$ | $\theta_{lin2}$ | $\theta_{max}$ | $\theta_{lin2}$ | $\theta_{max}$ |
| **8.5Z120-3E2W** | 0.027 | 0.031 | 0.023 | 0.036 | 0.028 | 0.031 | 0.028 | 0.034 | 0.027 | 0.031 | 0.023 | 0.036 | 0.031 | 0.031 | 0.031 | 0.034 |
| **8.5Z105-2E1W** | 0.034 | 0.034 | 0.029 | 0.035 | 0.030 | 0.034 | 0.030 | 0.035 | 0.034 | 0.034 | 0.029 | 0.035 | 0.034 | 0.034 | 0.034 | 0.035 |
| **8.5Z092-4E2W** | 0.022 | 0.031 | 0.021 | 0.032 | 0.024 | 0.030 | 0.024 | 0.031 | 0.022 | 0.031 | 0.021 | 0.032 | 0.030 | 0.030 | 0.030 | 0.031 |
| **8.5Z082-1E2W** | 0.021 | 0.031 | 0.021 | 0.029 | 0.024 | 0.030 | 0.024 | 0.029 | 0.023 | 0.031 | 0.024 | 0.029 | 0.030 | 0.030 | 0.030 | 0.029 |
| **8.5Z073-4E3W** | 0.022 | 0.024 | 0.021 | 0.024 | 0.021 | 0.024 | 0.021 | 0.023 | 0.024 | 0.024 | 0.024 | 0.024 | 0.024 | 0.025 | 0.024 | 0.024 |
| **8.5Z073-1E2W** | 0.016 | 0.022 | 0.015 | 0.024 | 0.020 | 0.021 | 0.020 | 0.022 | 0.016 | 0.022 | 0.014 | 0.024 | 0.023 | 0.022 | 0.023 | 0.023 |
| **8.5Z065-3E1W** | NaN | NaN | NaN | NaN | 0.018 | 0.020 | 0.018 | 0.020 | NaN | NaN | NaN | NaN | 0.020 | 0.020 | 0.020 | 0.020 |
| **8.5Z059-4E3W** | 0.016 | 0.019 | 0.016 | 0.020 | 0.020 | 0.019 | 0.020 | 0.020 | 0.017 | 0.019 | 0.018 | 0.020 | 0.022 | 0.019 | 0.022 | 0.020 |
| **8.5Z059-2E1W** | 0.022 | 0.022 | 0.020 | 0.020 | 0.020 | 0.022 | 0.020 | 0.020 | 0.021 | 0.022 | 0.020 | 0.020 | 0.021 | 0.023 | 0.021 | 0.021 |
| **8C097-2E3W** | 0.027 | 0.036 | 0.024 | 0.045 | 0.030 | 0.035 | 0.030 | 0.042 | 0.027 | 0.036 | 0.024 | 0.045 | 0.036 | 0.035 | 0.036 | 0.042 |
| **8C068-4E5W** | 0.019 | 0.030 | 0.017 | 0.041 | 0.022 | 0.029 | 0.022 | 0.036 | 0.011 | 0.030 | 0.004 | 0.041 | 0.029 | 0.029 | 0.029 | 0.036 |
| **8C068-1E2W** | 0.018 | 0.027 | 0.016 | 0.040 | 0.021 | 0.026 | 0.021 | 0.034 | 0.018 | 0.027 | 0.016 | 0.040 | 0.027 | 0.026 | 0.027 | 0.034 |
| **8C054-1E8W** | 0.014 | 0.026 | 0.014 | 0.028 | 0.017 | 0.024 | 0.017 | 0.026 | 0.017 | 0.026 | 0.017 | 0.028 | 0.021 | 0.025 | 0.021 | 0.027 |
| **8C043-5E6W** | 0.014 | 0.022 | 0.013 | 0.031 | 0.017 | 0.021 | 0.017 | 0.027 | 0.020 | 0.022 | 0.015 | 0.031 | 0.021 | 0.022 | 0.021 | 0.028 |
| **8C043-3E1W** | 0.013 | 0.021 | 0.012 | 0.033 | 0.016 | 0.020 | 0.016 | 0.028 | 0.017 | 0.021 | 0.014 | 0.033 | 0.021 | 0.021 | 0.021 | 0.029 |
| **12C068-9E5W** | 0.008 | 0.020 | 0.008 | 0.031 | 0.010 | 0.018 | 0.010 | 0.026 | 0.012 | 0.020 | 0.011 | 0.031 | 0.015 | 0.019 | 0.015 | 0.028 |
| **12C068-3E4W** | 0.009 | 0.017 | 0.009 | 0.028 | 0.013 | 0.016 | 0.013 | 0.023 | 0.014 | 0.017 | 0.012 | 0.028 | 0.018 | 0.017 | 0.018 | 0.024 |
| **10C068-2E1W** | 0.011 | 0.019 | 0.010 | 0.025 | 0.012 | 0.018 | 0.012 | 0.022 | 0.016 | 0.019 | 0.012 | 0.025 | 0.015 | 0.019 | 0.015 | 0.023 |
| **6C054-2E1W** | 0.019 | 0.045 | 0.019 | 0.048 | 0.023 | 0.041 | 0.023 | 0.043 | 0.019 | 0.045 | 0.019 | 0.048 | 0.039 | 0.041 | 0.039 | 0.043 |
| **4C054-1E2W** | 0.037 | 0.063 | 0.037 | 0.064 | 0.044 | 0.059 | 0.044 | 0.060 | 0.037 | 0.063 | 0.037 | 0.064 | 0.060 | 0.059 | 0.060 | 0.060 |
| **3.62C054-1E2W** | 0.035 | 0.066 | 0.035 | 0.066 | 0.038 | 0.064 | 0.038 | 0.064 | 0.035 | 0.066 | 0.035 | 0.066 | 0.066 | 0.064 | 0.066 | 0.064 |
| **11.5Z092-1E2W** | 0.014 | 0.019 | 0.014 | 0.019 | 0.016 | 0.019 | 0.016 | 0.019 | 0.014 | 0.019 | 0.014 | 0.019 | 0.016 | 0.019 | 0.016 | 0.019 |
| **11.5Z082-2E1W** | 0.012 | 0.017 | 0.012 | 0.018 | 0.016 | 0.016 | 0.016 | 0.017 | 0.013 | 0.017 | 0.012 | 0.018 | 0.016 | 0.016 | 0.016 | 0.017 |
| **11.5Z073-2E1W** | 0.011 | 0.016 | 0.010 | 0.020 | 0.013 | 0.016 | 0.013 | 0.018 | 0.014 | 0.016 | 0.011 | 0.020 | 0.015 | 0.016 | 0.015 | 0.018 |

(b) distortional buckling tests

| | EEEP-bilinear | | | | | | | | EEEP-trilinear | | | | | | | |
|---|---|---|---|---|---|---|---|---|---|---|---|---|---|---|---|---|
| | 1st | | | | 2nd | | | | 1st | | | | 2nd | | | |
| | 0.80F_peak | | 0.50F_peak | | 0.80F_peak | | 0.50F_peak | | 0.80F_peak | | 0.50F_peak | | 0.80F_peak | | 0.50F_peak | |
| | $\theta_{lin}$ | $\theta_{max}$ | $\theta_{lin}$ | $\theta_{max}$ | $\theta_{lin}$ | $\theta_{max}$ | $\theta_{lin}$ | $\theta_{max}$ | $\theta_{lin2}$ | $\theta_{max}$ | $\theta_{lin2}$ | $\theta_{max}$ | $\theta_{lin2}$ | $\theta_{max}$ | $\theta_{lin2}$ | $\theta_{max}$ |
| **D8.5Z120-4E1W** | 0.024 | 0.035 | 0.024 | 0.035 | 0.025 | 0.035 | 0.025 | 0.035 | 0.0274 | 0.035 | 0.027 | 0.035 | 0.027 | 0.035 | 0.027 | 0.0348 |
| **D8.5Z115-1E2W** | 0.020 | 0.039 | 0.018 | 0.044 | 0.023 | 0.038 | 0.023 | 0.040 | 0.0267 | 0.039 | 0.021 | 0.044 | 0.030 | 0.039 | 0.030 | 0.0409 |
| **D8.5Z092-3E1W** | 0.017 | 0.030 | 0.014 | 0.037 | 0.020 | 0.028 | 0.020 | 0.031 | 0.024 | 0.030 | 0.015 | 0.037 | 0.026 | 0.029 | 0.026 | 0.0319 |
| **D8.5Z082-4E3W** | 0.015 | 0.026 | 0.013 | 0.029 | 0.017 | 0.024 | 0.017 | 0.025 | 0.0225 | 0.026 | 0.015 | 0.029 | 0.023 | 0.026 | 0.023 | 0.0264 |
| **D8.5Z065-4E3W** | 0.015 | 0.023 | 0.014 | 0.026 | 0.017 | 0.022 | 0.017 | 0.024 | 0.0226 | 0.023 | 0.022 | 0.026 | 0.023 | 0.024 | 0.023 | 0.0255 |
| **D8.5Z065-1E2W-2** | 0.014 | 0.021 | 0.013 | 0.026 | 0.015 | 0.020 | 0.015 | 0.024 | 0.0173 | 0.021 | 0.015 | 0.026 | 0.018 | 0.021 | 0.018 | 0.0244 |
| **D8.5Z059-1W2E** | 0.010 | 0.021 | 0.010 | 0.028 | 0.013 | 0.020 | 0.013 | 0.024 | 0.0137 | 0.022 | 0.013 | 0.028 | 0.017 | 0.021 | 0.017 | 0.025 |
| **D11.5Z092-1E2W** | 0.013 | 0.019 | 0.013 | 0.019 | 0.018 | 0.018 | 0.018 | 0.018 | 0.0109 | 0.019 | 0.011 | 0.019 | 0.016 | 0.017 | 0.016 | 0.0174 |
| **D11.5Z082-5E4W** | 0.012 | 0.017 | 0.011 | 0.022 | 0.014 | 0.017 | 0.014 | 0.020 | 0.0163 | 0.017 | 0.014 | 0.022 | 0.016 | 0.017 | 0.016 | 0.0208 |
| **D8C097-5E4W** | 0.023 | 0.044 | 0.018 | 0.052 | 0.034 | 0.039 | 0.034 | 0.040 | 0.0229 | 0.044 | 0.014 | 0.053 | 0.044 | 0.040 | 0.044 | 0.0412 |
| **D8C085-2E1W** | 0.020 | 0.032 | 0.019 | 0.034 | 0.024 | 0.030 | 0.024 | 0.032 | 0.0237 | 0.032 | 0.022 | 0.034 | 0.031 | 0.031 | 0.031 | 0.0325 |
| **D8C068-6E7W** | 0.020 | 0.030 | 0.019 | 0.033 | 0.022 | 0.029 | 0.022 | 0.031 | 0.0286 | 0.030 | 0.023 | 0.033 | 0.028 | 0.030 | 0.028 | 0.0317 |
| **D8C054-7E6W** | 0.015 | 0.017 | 0.012 | 0.020 | 0.015 | 0.017 | 0.015 | 0.019 | 0.0162 | 0.017 | 0.013 | 0.020 | 0.016 | 0.017 | 0.016 | 0.0192 |
| **D8C045-1E2W** | 0.006 | 0.014 | 0.005 | 0.018 | 0.007 | 0.012 | 0.007 | 0.015 | 0.008 | 0.014 | 0.012 | 0.018 | 0.011 | 0.012 | 0.011 | 0.015 |
| **D8C043-4E2W** | 0.013 | 0.018 | 0.012 | 0.021 | 0.015 | 0.018 | 0.015 | 0.020 | 0.0175 | 0.018 | 0.014 | 0.022 | 0.018 | 0.019 | 0.018 | 0.0207 |
| **D8C033-1E2W** | 0.007 | 0.013 | 0.006 | 0.016 | 0.007 | 0.012 | 0.007 | 0.015 | 0.0074 | 0.013 | 0.006 | 0.016 | 0.010 | 0.012 | 0.010 | 0.0147 |
| **D12C068-10E11W** | 0.008 | 0.014 | 0.008 | 0.020 | 0.009 | 0.014 | 0.009 | 0.018 | 0.012 | 0.014 | 0.010 | 0.020 | 0.012 | 0.014 | 0.012 | 0.0188 |
| **D12C068-1E2W** | 0.006 | 0.017 | 0.006 | 0.017 | 0.009 | 0.013 | 0.009 | 0.013 | 0.0074 | 0.017 | 0.007 | 0.017 | 0.014 | 0.015 | 0.014 | 0.0147 |
| **D10C068-4E3W** | 0.006 | 0.014 | 0.006 | 0.019 | 0.008 | 0.013 | 0.008 | 0.017 | 0.0072 | 0.014 | 0.006 | 0.019 | 0.011 | 0.013 | 0.011 | 0.0169 |
| **D10C056-3E4W** | 0.010 | 0.017 | 0.010 | 0.021 | 0.012 | 0.016 | 0.012 | 0.019 | 0.0132 | 0.017 | 0.012 | 0.021 | 0.015 | 0.017 | 0.015 | 0.0199 |
| **D6C063-2E1W** | 0.026 | 0.036 | 0.027 | 0.035 | 0.028 | 0.035 | 0.028 | 0.034 | 0.0337 | 0.036 | 0.034 | 0.035 | 0.034 | 0.036 | 0.034 | 0.0353 |
| **D3.62C054-3E4W** | 0.037 | 0.059 | 0.029 | 0.065 | 0.033 | 0.061 | 0.033 | 0.061 | 0.0443 | 0.059 | 0.029 | 0.065 | 0.044 | 0.062 | 0.044 | 0.0615 |

A goal of this research is to parameterize the equivalent energy curves. DSM provides adequate strength prediction (e.g. see Fig 1f) therefore $M_{peak}$ is reasonably well predicted. DSM also provides pre-peak stiffness reduction (e.g., see Table 2) therefore $k_{\theta\text{-}prepeak}$ up to failure has a predictive method. Both $M_{peak}$ and $k_{\theta\text{-}prepeak}$ predictions are based on the cross-section slenderness. Figure 6 provides the results for the ductility: $\theta_{max}/\theta_{lin}$, for the EEEP-trilinear 1st method ($0.8M_{peak}$). These initial results indicate the correlation of ductility to cross-section slenderness may be challenging to establish.

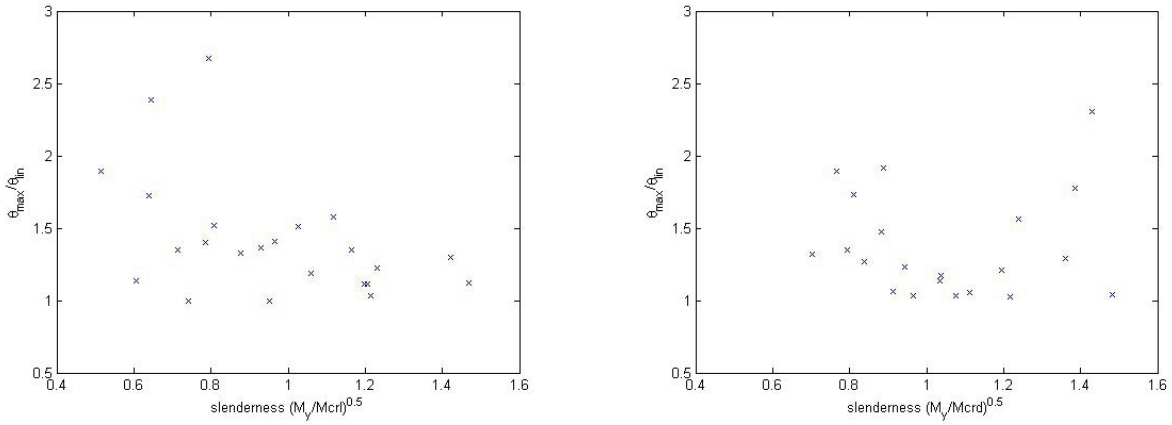


(a) local buckling tests (b) distortional buckling tests

Figure 6: Ductility as a function of cross-section slenderness

## 5. Discussion

Significant work remains to establish the ductility of cold-formed steel members and to parameterize that ductility into a useful design method that allows the ductility of arbitrary cold-formed steel members to be known and to be utilized in nonlinear modeling.

Subsequent to the testing of Yu and Schafer, Shifferaw and Schafer (2011) explored inelastic bending reserve in these same specimens. Further, they augmented the testing with additional nonlinear shell finite element collapse on sections with low cross-section slenderness. The strain capacity in these sections was well correlated to cross-section slenderness. This suggests that these members are a good candidate for understanding the relationship between ductility and cross-section slenderness and studies in this direction are underway.

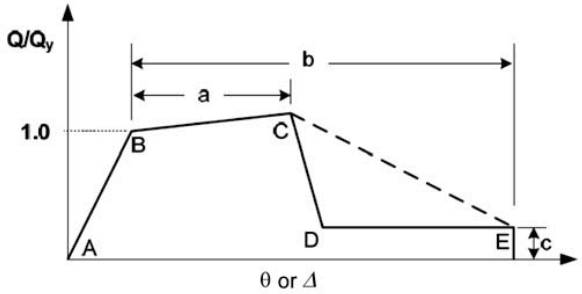


Figure 7: Nonlinear Static $M$-$\theta$ model from PEER/ATC (2010)

The bilinear and trilinear EEEP models explored in this paper do not allow for post-peak stiffness degradation. This is a significant limitation and is not consistent with the observed response from the tests (Fig. 1g and h) where significant post-peak loss occurs over a small range of rotation. The $M$-$\theta$ models of ASCE 41 (2007) or PEER/ATC (2010) as depicted in Figure 7 need to be explored. In particular, the normalized strength loss from C to D is anticipated to be more closely correlated to the cross-section slenderness. Work in this direction is also currently underway.

Existing tests and models only cover monotonic, static, loading. Stiffness degradation under repeated cycles, etc. is unknown. Recently the senior author worked with the American Iron and Steel Institute to establish a small project to provide this data. The project was awarded to Professors Moen and Eatherton at Virginia Tech and will supply much needed data on this phenomenon. The project will be coordinated with the cold-formed steel seismic engineering project underway at Johns Hopkins (cfs-nees: www.ce.jhu.edu/cfsnees).

## 6. Conclusions

As the use of cold-formed steel members and systems advances so must the analysis capabilities that support that advancement. This paper provides work towards providing the stiffness, both before and after the peak strength, for cold-formed steel members. Existing test data on cold-formed steel beams, lipped channel and lipped zees, tested under monotonic, static conditions and failing in local and distortional buckling are utilized for the analysis presented herein. Comparison of the pre-peak stiffness degradation, that results due to cross-section slenderness, is provided for the effective width method and the direct strength method. Both methods have a high variance when compared to the testing. The mean performance of the direct strength method expressions for stiffness degradation is better than that of the effective width method, and the expressions are arguably simpler. Member ductility and post-peak performance is characterized for the tests using variations on equivalent energy elastic-plastic models (both a bilinear and trilinear model). The characterization is only a partial success, as due to significant strength degradation, in some cases the elastic-plastic model cannot be equated to the recorded energy. Further, the measured ductility does not obviously correlate with cross-section slenderness. A number of efforts, discussed herein, are underway to address these issues – most notably the exploration of a multi-linear response curve that includes significant post-peak strength degradation.

## 5. Acknowledgments

This material is based upon work supported by the National Science Foundation under Grant No. 1041578. Any opinions, findings, and conclusions or recommendations expressed in this material are those of the authors and do not necessarily reflect the views of the National Science Foundation

## References

American Iron and Steel Institute (AISI). (2007). *North American Specification for the Design of Cold-Formed Steel Structural Members; and 2007 edition: Commentary on the Specification*, Washington, D.C.

American Iron and Steel Institute (AISI). (2007). *Supplement 2007 to the North American Specification for the Design of Cold-Formed Steel Structural Members, 2007 edition, Appendix 1, Design of Cold-Formed Steel Structural Members Using Direct Strength Method*, Washington, D.C.

American Society of Civil Engineers (ASCE/SEI 41-06). (2007). *Seismic Rehabilitation of Existing Buildings*, Reston, Virginia

Branston, A.E., Boudreault, F.A., Chen, C.Y., and Rogers, C.A. (2006). "Light-gauge steel frame – wood structural panel shear wall design method." *Canadian Journal of Civil Engineering*, NRC, 872-889.

CFS. (2010) Cold-Formed Steel Component Design Software. *RGS Software Inc*.

Park, R. (1988). "Ductility Evaluation from Laboratory and Analytical Testing." *9th World Conference on Earthquake Engineering*, Tokyo-Kyoto, Japan, Vol.VIII.

PEER/ATC (2010). *Modeling and acceptance criteria for seismic design and analysis of tall buildings*, PEER/ATC 72-1 Report, Applied Technology Council, Redwood City, CA, October 2010.

Schafer, B.W. (2006). "Review: Direct Strength Method of Cold-Formed Steel Member Design." *Stability and Ductility of Steel Structures*, Lisbon, Portugal.

Schafer, B.W., Peköz, T. (1998). "Direct Strength Prediction of Cold-Formed Steel Members using Numerical Elastic Buckling Solutions." *14th Int'l. Spec. Conf. on Cold-Formed Steel Structures*, St. Louis, Missouri.

Shifferaw, Y., Schafer, B.W. (2011). "Inelastic Bending Capacity of Cold-Formed Steel Members." ASCE, *Journal of Structural Engineering*. Submitted for publication, currently under review

Yu, C., Schafer, B.W. (2003). "Local buckling Test on Cold-Formed Steel Beams." *Journal of Structural Engineering.* ASCE, 129 (12) 1596-1606.

Yu, C, Schafer, B.W., (2006). "Distortional buckling tests on cold formed steel beams." *Journal of Structural Engineering*, ASCE, 515-528.

Ziemian, R.D. (2010). Guide to Stability Design Criteria for Metal Structures, Chapter 13: Thin-Walled Metal Construction, 6th Edition, *Wiley & Sons Inc*.